

In-Plane Flexoelectricity in Two-Dimensional D_{3d} CrystalsMatteo Springolo,¹ Miquel Royo^{1,*} and Massimiliano Stengel^{1,2,†}¹*Institut de Ciència de Materials de Barcelona (ICMAB-CSIC), Campus UAB, 08193 Bellaterra, Spain*²*ICREA—Institució Catalana de Recerca i Estudis Avançats, 08010 Barcelona, Spain* (Received 31 March 2023; revised 31 July 2023; accepted 25 October 2023; published 8 December 2023)

We predict a large in-plane polarization response to bending in a broad class of trigonal two-dimensional crystals. We define and compute the relevant flexoelectric coefficients from first principles as linear-response properties of the undistorted layer by using the primitive crystal cell. The ensuing response (evaluated for SnS₂, silicene, phosphorene, and RhI₃ monolayers and for a hexagonal BN bilayer) is up to 1 order of magnitude larger than the out-of-plane components in the same material. We illustrate the topological implications of our findings by calculating the polarization textures that are associated with a variety of rippled and bent structures. We also determine the longitudinal electric fields induced by a flexural phonon at leading order in amplitude and momentum.

DOI: 10.1103/PhysRevLett.131.236203

The electromechanical properties of two-dimensional (2D) materials have generated considerable research interest recently due to their potential application in flexible, stretchable, foldable, and wearable nanoscale devices [1–3]. Materials design paradigms have traditionally relied on piezoelectricity, whose in-plane components are active in a broad variety of hexagonal monolayers [4–7]. More recently, flexoelectricity (the generation of a macroscopic polarization or voltage in response to a strain gradient) has emerged as an appealing higher-order alternative, thanks to its favorable scaling with decreasing sample size [8]. Indeed, 2D materials can sustain large bending deformations without fracturing [9], which in principle should enable a large flexoelectric response.

Flexoelectricity in 2D materials has been mostly studied as an out-of-plane dipolar response due to a flexural (bending) deformation. Several studies of graphene, BN, phosphorene, transition-metal dichalcogenides, and related materials have reported a great variety of magnitudes and signs for the relevant flexoelectric coefficient, sometimes with significant mutual disagreement. On the experimental side [10–15], such inconsistencies likely originate from the difficulty in extracting the intrinsic response of the 2D monolayer from the measured signal. The scatter in the theoretical values, on the other hand, can be either traced back to the broad variety of methods that were used in each case, ranging from first-principles techniques [16–23] to classical [24–26] and machine-learning [27,28] force fields, or to the technical subtleties in defining the dipole moment of a curved surface. These difficulties can now be largely avoided via a publicly available [29–31] linear-response implementation [32], which is aimed at providing reference first-principles values for the direct and converse flexoelectric effect in arbitrary 2D systems.

While the aforementioned out-of-plane response is universal, it turns out to be small in many materials. In the present Letter, we investigate the in-plane polarization response to a flexural deformation instead, which we indicate as “unconventional” as it is typically ruled out in three-dimensional (3D) crystals of sufficiently high symmetry. The effect, illustrated in Figs. 1(a) and 1(b), is linear in the layer curvature, and therefore differs from the nonlinear one predicted in monolayer *h*-BN [33] some time ago. It is active in a surprisingly broad class of 2D systems, including many of the best studied materials. Interestingly, for materials with D_{3d} point symmetry (space groups $P\bar{3}m1$ and $P\bar{3}1m$), the amplitude of the polarization response is insensitive to the bending direction, while its orientation continuously rotates in plane, with an angular periodicity that matches the threefold axis of the flat configuration [Figs. 1(b) and 1(c)]. Apart from the obvious practical interest for energy-harvesting applications [34], such an effect is important for fundamental reasons as well. Most notably, it leads to a broad range of topologically nontrivial polarization textures in rippled and bent geometries, including vortices and antivortices and spontaneously polarized tubes. Moreover, it endows flexural phonons with longitudinal electric fields (and hence, with a long-ranged contribution to the electron-phonon Hamiltonian), which may significantly contribute to the mobility in the low-temperature regime [35–38].

Our goal is to express the flexoelectric coefficients in terms of a “strict-2D” model of the layer, as a surface polarization [39] response to curvature. The geometry of the problem is conveniently specified via a vector function of two variables $\mathbf{r} = \mathbf{r}(u, v)$, where \mathbf{r} is a point in 3D space in the deformed configuration, and uv refers to a local parametrization of the reference state [40]. Then, the Cartesian components of the surface polarization can be

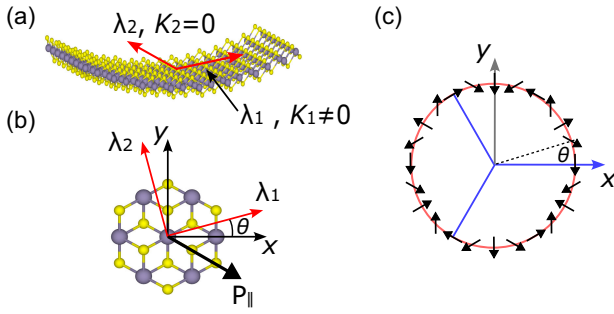


FIG. 1. (a) Schematic illustration of a slab bent along the (principal) direction λ_1 with a (principal) curvature K_1 . Red arrows indicate the principal bending directions. (b) 2D geometry for SnS_2 . θ indicates the angle between the axis x and the principal direction λ_1 . The induced in-plane polarization P_{\parallel} is indicated for an angle $\theta = 15^\circ$. (c) Orientation evolution of the induced in-plane polarization with respect to the bending direction (θ). Threefold symmetry is highlighted by the use of blue lines.

expressed as $\mathbf{P} = (P_u \mathbf{r}_u + P_v \mathbf{r}_v) / \sqrt{g}$, where $\mathbf{r}_\alpha = \partial \mathbf{r} / \partial \xi^\alpha$ are deformation gradients, $\xi^\alpha = u, v$ are curvilinear coordinates, and g is the determinant of the (2D) metric tensor $g_{\alpha\beta}$. (From now on, we shall use greek indices for the in-plane uv directions.) The local curvature, in turn, is well described by the matrix elements of the second fundamental form $b_{\alpha\beta} = \mathbf{r}_{\alpha\beta} \cdot \mathbf{n}$, where the subscripts $\alpha\beta$ stand for (second) differentiation with respect to u, v , and $\mathbf{n}(u, v)$ is the normal to the oriented surface. (We choose it in such a way that $\mathbf{r}_u, \mathbf{r}_v$, and \mathbf{n} form a right-handed set.) This, in principle, allows us to write the flexoelectric coefficient in the reference configuration as derivatives of P_α with respect to $b_{\beta\gamma}$.

Real materials, however, are “quasi-2D”; i.e., they are extended in plane but have a nonvanishing thickness along the surface normal (z). Consequently, in practical calculations one needs to assume a 3D-3D mapping $\mathbf{r}(u, v, z)$, involving a region of space that is thin but finite along z . We shall set $\mathbf{r}_z = \mathbf{n}$ henceforth; then, the matrix elements of \mathbf{b} coincide with the Christoffel symbol $\Gamma_{z\beta\gamma}$ and relate to the z gradient of the metric as follows:

$$b_{\beta\gamma} = \Gamma_{z\beta\gamma} = -\frac{1}{2} \frac{\partial g_{\beta\gamma}}{\partial z}. \quad (1)$$

The latter two quantities, with the physical meaning of strain gradients, are uniform along z and are therefore the appropriate macroscopic variable to describe curvature in a quasi-2D context [32]. The strict-2D limit is eventually recovered by integrating along z the microscopic polarization response.

In the linear regime, the gradient of the metric coincides with the “type-II” representation of the strain-gradient tensor $\frac{1}{2} \partial g_{\beta\gamma} / \partial z \simeq \partial \varepsilon_{\beta\gamma} / \partial z = \varepsilon_{\beta\gamma,z}$, where $\varepsilon_{\beta\gamma}$ is the symmetrized infinitesimal strain. Thus, we define the relevant

flexoelectric coefficients as first derivatives of the surface polarization \mathbf{P} with respect to $\varepsilon_{\beta\gamma,z}$,

$$P_\alpha = \mu_{\alpha z, \beta\gamma}^{2D} \varepsilon_{\beta\gamma,z}. \quad (2)$$

The derivative is intended to be taken at zero macroscopic electric field corresponding to short-circuit boundary conditions; this is the most natural choice given the extended nature of the crystal in the x - y plane. Our choice of notation is motivated by the obvious analogy with the definition of the type-II flexoelectric coefficients in 3D [41]. One should keep in mind, however, that here \mathbf{P} is defined as a charge per unit length; consequently, the flexoelectric coefficients $\mu_{\alpha z, \beta\gamma}^{2D}$ have the dimension of a charge.

A necessary condition for any of these coefficients to be nonzero is the lack of a z -oriented mirror plane; similarly, xy inversion cannot be a symmetry, as the tensorial dependence on the in-plane indices is odd. While our theory is valid in the most general case, in the following we focus on a subset of these materials that have the highest symmetry compatible with the above criteria. More specifically, we consider crystals with a z -oriented threefold axis, space inversion symmetry, and a vertical mirror plane (space groups $\bar{P}3m1$ and $\bar{P}31m$, D_{3d} point group). Within this set, there are only three nonzero in-plane components of the type $\mu_{\alpha z, \beta\gamma}^{2D}$. Assuming a zy mirror plane (x is the armchair direction in $\bar{P}31m$ crystals, and zigzag in $\bar{P}3m1$), they are related to each other as

$$\mu_{yz,yy}^{2D} = -\mu, \quad \mu_{yz,xx}^{2D} = \mu_{xz,xy}^{2D} = \mu, \quad (3)$$

where μ is the only independent component. This choice leaves the freedom for two nonequivalent configurations related by a $z \rightarrow -z$ mirror operation or, equivalently, by a rotation of $(2n+1)\pi/3$ about the threefold axis. The two structural variants have opposite μ coefficient, which results in a sign ambiguity unless the atomic positions are fully specified; our data refer to the structures shown in Fig. 2 and reported in the Supplemental Material [42].

To see the practical implications of Eq. (3), it is convenient to represent the strain-gradient components in terms of principal curvatures (K_i) and directions (λ_i) as $\varepsilon_{\beta\gamma,z} = \sum_i K_i \lambda_i^\beta \lambda_i^\gamma$. Then, by writing $\lambda_1 = [\cos(\theta), \sin(\theta)]$ and $\lambda_2 = [-\sin(\theta), \cos(\theta)]$ in terms of the angle θ [Fig. 1(b)], we find

$$\mathbf{P}_{\parallel}(\theta) = \mu(\sin(3\theta)\lambda_1 - \cos(3\theta)\lambda_2)(K_1 - K_2). \quad (4)$$

Remarkably, the modulus of the linearly induced polarization is θ independent $P_{\parallel}(\theta) = |\mu(K_1 - K_2)|$ and only depends on the difference between the principal curvatures. (The case $K_1 = K_2$ corresponds to a deformation with spherical symmetry, which locally preserves the threefold axis of the structure and therefore cannot produce an

in-plane \mathbf{P} .) On the other hand, the polarization direction continuously rotates in plane with an angular periodicity that is 3 times that of the principal axes. This means that the induced polarization is manifestly invariant with respect to $\theta \rightarrow \theta \pm m2\pi/3$ [Fig. 1(c)] with integer m , again consistent with the D_{3d} symmetry of the crystal.

Such a peculiar angular dependence of the polarization response is common to many electromechanical properties of hexagonal layers. For example, an analogous behavior was found in Naumov *et al.* [33] for the polarization induced at the second order in the curvature in a monolayer of h -BN. Most importantly, Eq. (3) matches the internal symmetries of the piezoelectric tensor $e_{\alpha\beta\gamma}$ in BN and other isostructural materials (e.g., MoS_2) with a z -mirror plane but no space inversion. Indeed, for these materials we have

$$e_{y,yy} = -E, \quad e_{y,xx} = e_{x,xy} = E, \quad (5)$$

and the induced polarization can be written exactly as in Eq. (4), provided that we replace the principal curvatures K_i with the principal stretches ε_i and the flexoelectric constant μ with E . This analogy suggests that a flexoelectric effect with the characteristics of Eq. (4) should be present in a bilayer of h -BN and related compounds, provided that they are appropriately stacked (AA' or AB') in order to recover D_{3d} symmetry. In this case, within the assumption that the layers do not interact significantly, one expects

$$\mu \simeq Eh, \quad (6)$$

where h is the interlayer distance. Equation (6) generalizes the results of Ref. [34] to a generic flexural deformation; here, we shall use it as validation of our computational method by including the h -BN bilayer in our materials test set.

We shall focus now on the first-principles calculation of $\mu_{\alpha z, \beta \gamma}^{2D}$. Our calculations are performed within the local-density approximation as implemented in the ABINIT package [30,51]. We represent the 2D crystals by using the primitive surface cells shown in Fig. 2; we assume periodic boundary conditions along z , with a reasonably large separation L between images. Following Ref. [32], we express the flexoelectric coefficients in terms of a clamped-ion (CI) and a lattice-mediated (LM) contributions $\mu_{\alpha z, \beta \gamma}^{2D} = \mu_{\alpha z, \beta \gamma}^{2D, \text{CI}} + \mu_{\alpha z, \beta \gamma}^{2D, \text{LM}}$. We find [42]

$$\mu_{\alpha z, \beta \gamma}^{2D, \text{CI}} = -\frac{1}{2} \left[\mu_{\alpha \gamma, z \beta}^{\text{II, CI}} + \mu_{\alpha \beta, z \gamma}^{\text{II, CI}} + \sum_{\kappa} \tau_{\kappa z} \left(\bar{P}_{\alpha, \kappa \gamma}^{(1, \beta)} + \bar{P}_{\alpha, \kappa \beta}^{(1, \gamma)} \right) \right], \quad (7)$$

where $\mu_{\alpha \gamma, z \beta}^{\text{II, CI}}$ is the 3D clamped-ion flexoelectric coefficient of the supercell in type-II form [41], τ_{κ} is the undistorted

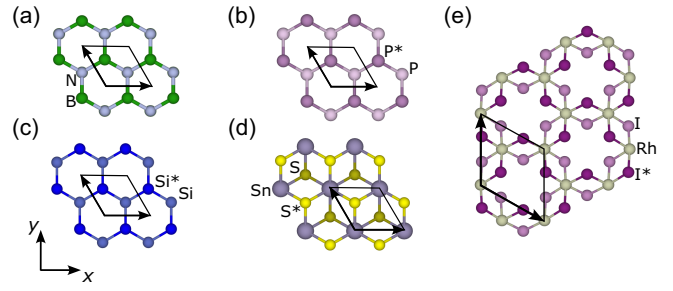


FIG. 2. Top view of the crystal structures employed in the linear-response calculations for the materials considered: h -BN bilayer (a), blue phosphorene (b), silicene (c), SnS_2 (d), and RhI_3 (e). The primitive cell is highlighted. Upper and lower atoms of the same type are indicated with the same color but different shade. Upper atoms are explicitly indicated with an asterisk.

location of sublattice κ , and $\bar{\mathbf{P}}_{\kappa \gamma}^{(1, \beta)}$ is the first-order spatial dispersion (along β) of the macroscopic polarization response to a displacement of the atom κ along the direction γ [31,41]. Similarly, we write the LM contribution as

$$\mu_{\alpha z, \beta \gamma}^{2D, \text{LM}} = \frac{1}{S} Z_{\kappa \rho}^{(\alpha)} \mathcal{L}_{\rho z, \beta \gamma}^{\kappa}, \quad (8)$$

where $Z_{\kappa \rho}^{(\alpha)}$ are the Born effective charges, and \mathcal{L} is the flexoelectric internal-relaxation tensor of the isolated layer as defined and calculated in Ref. [32].

All ingredients in Eqs. (7) and (8) can be readily calculated with the linear-response and long-wave [29–31] modules of ABINIT. Computational parameters and convergence tests are described in the Supplemental Material [42], where we also discuss and prove the following formal results: (i) the contribution of the metric variation to $\mu_{\alpha z, \beta \gamma}^{2D}$ vanishes, unlike the out-of-plane case studied in Ref. [32]; (ii) the type-II 2D coefficients described here directly relate to the macroscopic 3D coefficients of the supercell in type-I [41] form via $\mu_{\alpha z, \beta \gamma}^{2D} = -L \mu_{\alpha z, \beta \gamma}^{\text{I}}$, without the need for calculating additional terms; (iii) modifying the electrostatic kernel to account for the 2D nature of the problem [52] is unnecessary as long as the macroscopic dielectric tensor is diagonal. (This is the case for all materials considered here.) Note that the $\mu_{\alpha z, \beta \gamma}^{2D}$ coefficients that we define and calculate are intrinsic properties of the extended 2D crystal; therefore, they are applicable to modeling an arbitrary rippled or bent structure, as we shall illustrate (and substantiate with explicit validation tests) shortly.

As a first consistency check of our method, we shall prove that we recover Eq. (6) and, therefore, the results of Ref. [34] in the case of the h -BN bilayer. To perform this test, we first calculate the value of the piezoelectric constant for an isolated h -BN monolayer, obtaining $E^{\text{CI}} = 0.1230$ e/bohr and $E^{\text{LM}} = -0.0810$ e/bohr for the CI and LM parts, respectively, yielding a total $E = 0.0420$ e/bohr. Then, we relax the geometry of an AA'-stacked bilayer, consistent with the geometry used in Ref. [34], obtaining an

TABLE I. Characteristic 2D flexocoefficients due to a flexural deformation. Three leftmost columns show the clamped-ion (CI), lattice-mediated (LM), and relaxed-ion (RI) contributions to the in-plane response $\mu_{yz,xx}^{2D}$. The fourth column shows the out-of-plane RI response $\mu_{zz,xx}^{2D}$. Results are provided in units of electronic charge.

| | $\mu_{yz,xx}^{2D}$ | | | $\mu_{zz,xx}^{2D}$ |
|------------------|--------------------|---------|---------|--------------------|
| | CI | LM | RI | RI |
| Si | 0.0299 | 0.0000 | 0.0299 | 0.0032 |
| BN (bilayer) | 0.7569 | -0.4947 | 0.2622 | -0.0304 |
| (Blue) P | 0.0721 | 0.0000 | 0.0721 | 0.0212 |
| SnS ₂ | 0.1257 | -0.2263 | -0.1006 | 0.0198 |
| RhI ₃ | -0.1766 | 0.0102 | -0.1664 | -0.0062 |

interlayer distance of $h = 6.14$ bohr (the experimental bulk spacing is 6.2928 bohr [53]). By plugging these values into Eq. (6), we obtain $\mu^{CI} = 0.7548 e$, $\mu^{LM} = -0.4970 e$, and $\mu = 0.2577 e$, in excellent agreement with the results reported in Table I.

The calculated 2D in-plane flexocoefficients ($\mu_{\alpha z, \beta \gamma}^{2D}$) of silicene, blue phosphorene, SnS₂, and RhI₃ monolayers, as well as of the h -BN bilayer with AA' stacking, are shown in Table I along with the corresponding out-of-plane ones. (The latter calculated as $\mu_{zz, \beta \beta}^{2D} = \epsilon_0 \varphi$ from the flexovoltage φ as defined in Ref. [32].) Interestingly, our results indicate that the in-plane flexoelectric response is much larger than the out-of-plane one, in several cases about 1 order of magnitude larger. This trend is common to all the studied materials despite the systematic sign reversal observed for the CI and LM contributions; both are generally comparable in module, except for RhI₃ where the LM term is 1 order of magnitude smaller.

To get a flavor of how large the predicted effect is, we can compare it to the nonlinear one described by Naumov *et al.* [33], which involves the in-plane polarization response to the square of the local curvature. Of course, the coefficients are not directly comparable, as they occur at different orders in the deformation amplitude; however, we can estimate a critical radius of curvature (R^*) at which the respective magnitudes of the induced polarization become similar. Extracting a second-order coefficient from the numbers provided in Ref. [33] and employing the linear-order coefficient for the h -BN bilayer, we obtain an unrealistically small value of $R^* \sim 0.75$ bohr, with the linear effect prevailing at any $R > R^*$. For instance, Naumov *et al.* obtained induced polarizations $P \sim 0.013 e/\text{bohr}$ for an h -BN monolayer corrugated along a zigzag direction with an average radius $R \sim 6.7$ bohr and at a CI level. Instead, taking our CI coefficient for the h -BN bilayer (Table I), the present linear effect reaches the same magnitude at curvature radii $R \sim 60$ bohr. At deformation regimes that are currently attainable in a laboratory [54] ($R \sim 10 \mu\text{m}$), the linear response of the bilayer is stronger

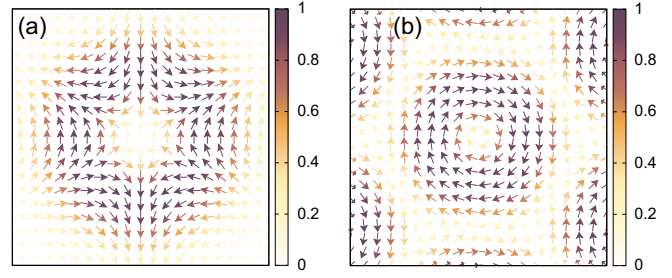


FIG. 3. Polarization textures associated with two different ripple patterns. (a) Gaussian bump of the type $z = A e^{-(x^2+y^2)/\sigma^2}$. (b) Periodic pattern of the type $z = A \sum_{i=1}^3 \sin(\mathbf{q}_i \cdot \mathbf{r})$, with $\mathbf{q}_1 = q(1, 0, 0)$, $\mathbf{q}_2 = q(-1/2, \sqrt{3}/2, 0)$, $\mathbf{q}_3 = q(-1/2, -\sqrt{3}/2, 0)$, and $q = 2\pi/L$. The arrows indicate the polarization direction; its amplitude (in units of $|P^{\max}| = 1.48A\mu/\sigma^2$ and $|P^{\max}| = 1.75A\mu q^2$, respectively) is defined by the color scale.

than the nonlinear one of the monolayer by 5 orders of magnitude.

A direct outcome of the predicted flexoelectric coupling is the emergence of topologically nontrivial in-plane polarization textures in arbitrary rippled states. To illustrate this, in Fig. 3(a) we show the in-plane polarization field that results from an isolated Gaussian-shaped bump consisting in a textbook antivortex structure with a topological charge (winding number) [55] of $Q = -2$. In Fig. 3(b), we consider a periodic deformation pattern consisting of three superimposed sinusoidal ripples with threefold symmetry; the result is a hexagonal lattice of clockwise vortices ($Q = 1$). By playing with these two examples [42], we could obtain a whole range of patterns, including an array of monopoles, and in-plane textures that closely resemble those of Ref. [56]. All these structures could, in principle, be characterized experimentally by optical means (e.g., via second harmonic generation [57]).

As a corollary of the above, our theory predicts an axial spontaneous polarization in nanotubes made of 2D trigonal crystals. In particular, a nanotube constructed by folding a layer along λ_1 acquires a linear polarization in the form

$$P^{1D} = -2\pi\mu \cos(3\theta), \quad (9)$$

independent of its radius R . To test this result, we perform explicit ground-state density functional theory calculations of zigzag SnS₂ nanotubes via VASP.5.4. [58–61]. We find [42] excellent agreement between the computed Berry phase polarization of the tube and the predictions of Eq. (9). Note that a circulating (azimuthal) component of the polarization, of amplitude $P_\theta = \mu/R \sin(3\theta)$, is generally also present. P_θ is largest for $\theta = (2n+1)\pi/6$, with integer n , where Eq. (9) yields a vanishing result. For $\theta \neq n\pi/6$, the two components coexist, and the polarization field becomes chiral.

Another central consequence of our theory is that the present mechanism endows flexural phonons with

longitudinal electric fields, which may be of considerable importance in the context of electron-phonon couplings. For a propagation direction $\mathbf{q} = q\lambda_1$, a combination of Eqs. (7) and (8) with the formalism developed in Refs. [37,38,52] leads to a macroscopic electrostatic contribution to the scattering potential (and hence, to the diagonal electron-phonon matrix elements) in the form

$$V^{\parallel}(\mathbf{q}) = -2\pi i q^2 \mu \sin(3\theta) + O(q^3). \quad (10)$$

An independent proof of this formula based on the formalism of Ref. [52] is provided in the Supplemental Material [42]. As the ensemble average of the flexural phonon amplitude diverges at any temperature [35,36] for $\mathbf{q} \rightarrow 0$, we suspect that Eq. (10) may contribute significantly to electron transport; a verification of this point will be an interesting topic for future studies.

To summarize, we have predicted and numerically demonstrated the existence of an in-plane polarization response to a flexural deformation in trigonal 2D monolayers. We have also discussed the topological implications of our results in a variety of rippled and bent geometries. In addition, we have demonstrated the relevance of the effect in dealing with the long-range electrostatic fields induced by a flexural phonon, with potential implications for electron-phonon physics. We hope that our results will stimulate experimental efforts at detecting the effects we describe here, e.g., along the lines that we suggest in Sec. 8 of Ref. [42].

We acknowledge support from Ministerio de Ciencia e Innovación (MICINN-Spain) through Grants No. PID2019-108573GB-C22 and Severo Ochoa FUNFUTURE center of excellence (CEX2019-000917-S); from Generalitat de Catalunya (Grant No. 2021 SGR 01519); and from the European Research Council (ERC) under the European Union's Horizon 2020 research and innovation program (Grant Agreement No. 724529). Part of the calculations were performed at the Supercomputing Center of Galicia.

*mroyo@icmab.es

†mstengel@icmab.es

- [1] Feng Ru Fan, Wei Tang, and Zhong Lin Wang, Flexible nanogenerators for energy harvesting and self-powered electronics, *Adv. Mater.* **28**, 4283 (2016).
- [2] Mingzeng Peng, Jiadong Cheng, Xinxin Zheng, Jingwen Ma, Ziyao Feng, and Xiankai Sun, 2D-materials-integrated optoelectromechanics: Recent progress and future perspectives, *Rep. Prog. Phys.* **86**, 026402 (2023).
- [3] Mukesh Pandey, Cheeranjiv Pandey, Rajeev Ahuja, and Rakesh Kumar, Straining techniques for strain engineering of 2D materials towards flexible straintronic applications, *Nano Energy* **109**, 108278 (2023).
- [4] Wenzhuo Wu, Lei Wang, Yilei Li, Fan Zhang, Long Lin, Simiao Niu, Daniel Chenet, Xian Zhang, Yufeng Hao, Tony

- F. Heinz, James Hone, and Zhong Lin Wang, Piezoelectricity of single-atomic-layer MoS₂ for energy conversion and piezotronics, *Nature (London)* **514**, 470 (2014).
- [5] Hanyu Zhu, Yuan Wang, Jun Xiao, Ming Liu, Shaomin Xiong, Zi Jing Wong, Ziliang Ye, Yu Ye, Xiaobo Yin, and Xiang Zhang, Observation of piezoelectricity in free-standing monolayer MoS₂, *Nat. Nanotechnol.* **10**, 151 (2014).
- [6] Ruixiang Fei, Wenbin Li, Ju Li, and Li Yang, Giant piezoelectricity of monolayer group IV monochalcogenides: SnSe, SnS, GeSe, and GeS, *Appl. Phys. Lett.* **107**, 173104 (2015).
- [7] Liang Dong, Jun Lou, and Vivek B. Shenoy, Large in-plane and vertical piezoelectricity in Janus transition metal dichalcogenides, *ACS Nano* **11**, 8242 (2017).
- [8] Thanh D. Nguyen, Sheng Mao, Yao-Wen Yeh, Prashant K. Purohit, and Michael C. McAlpine, Nanoscale flexoelectricity, *Adv. Mater.* **25**, 946 (2013).
- [9] Deji Akinwande *et al.*, A review on mechanics and mechanical properties of 2D materials—graphene and beyond, *Extreme Mech. Lett.* **13**, 42 (2017).
- [10] Christopher J. Brennan, Rudresh Ghosh, Kalhan Koul, Sanjay K. Banerjee, Nanshu Lu, and Edward T. Yu, Out-of-plane electromechanical response of monolayer molybdenum disulfide measured by piezoresponse force microscopy, *Nano Lett.* **17**, 5464 (2017).
- [11] Christopher J. Brennan, Kalhan Koul, Nanshu Lu, and Edward T. Yu, Out-of-plane electromechanical coupling in transition metal dichalcogenides, *Appl. Phys. Lett.* **116**, 053101 (2020).
- [12] Leo J. McGilly *et al.*, Visualization of oimré superlattices, *Nat. Nanotechnol.* **15**, 580 (2020).
- [13] Md Farhadul Haque, Peter Snapp, Jin Myung Kim, Michael Cai Wang, Hyung Jong Bae, Chullhee Cho, and SungWoo Nam, Strongly enhanced electromechanical coupling in atomically thin transition metal dichalcogenides, *Mater. Today* **47**, 69 (2021).
- [14] Liang Sun, B. Javvaji, Chunli Zhang, Xiaoying Zhuang, and Weiqiu Chen, Effect of flexoelectricity on a bilayer molybdenum disulfide Schottky contact, *Nano Energy* **102**, 107701 (2022).
- [15] Hiroyuki Hirakata, Yasuyuki Fukuda, and Takahiro Shimada, Flexoelectric properties of multilayer two-dimensional material MoS₂, *J. Phys. D* **55**, 125302 (2021).
- [16] Traian Dumitrică, Chad M. Landis, and Boris I. Yakobson, Curvature-induced polarization in carbon nanoshells, *Chem. Phys. Lett.* **360**, 182 (2002).
- [17] Sergei V. Kalinin and Vincent Meunier, Electronic flexoelectricity in low-dimensional systems, *Phys. Rev. B* **77**, 033403 (2008).
- [18] Wenhao Shi, Yufeng Guo, Zhuhua Zhang, and Wanlin Guo, Flexoelectricity in monolayer transition metal dichalcogenides, *J. Phys. Chem. Lett.* **9**, 6841 (2018).
- [19] Wenhao Shi, Yufeng Guo, Zhuhua Zhang, and Wanlin Guo, Strain gradient mediated magnetism and polarization in monolayer VSe₂, *J. Phys. Chem. C* **123**, 24988 (2019).
- [20] T. Pandey, L. Covaci, and F. M. Peeters, Tuning flexoelectricity and electronic properties of zig-zag graphene nanoribbons by functionalization, *Carbon* **171**, 551 (2021).
- [21] T. Pandey, L. Covaci, M. V. Milošević, and F. M. Peeters, Flexoelectricity and transport properties of phosphorene

- nanoribbons under mechanical bending, *Phys. Rev. B* **103**, 235406 (2021).
- [22] David Codony, Irene Arias, and Phanish Suryanarayana, Transversal flexoelectric coefficient for nanostructures at finite deformations from first principles, *Phys. Rev. Mater.* **5**, 030801 (2021).
- [23] Shashikant Kumar, David Codony, Irene Arias, and Phanish Suryanarayana, Flexoelectricity in atomic monolayers from first principles, *Nanoscale* **13**, 1600 (2021).
- [24] Xiaoying Zhuang, Bo He, Brahmanandam Javvaji, and Harold S. Park, Intrinsic bending flexoelectric constants in two-dimensional materials, *Phys. Rev. B* **99**, 054105 (2019).
- [25] Brahmanandam Javvaji, Bo He, Xiaoying Zhuang, and Harold S. Park, High flexoelectric constants in Janus transition-metal dichalcogenides, *Phys. Rev. Mater.* **3**, 125402 (2019).
- [26] Yida Yang, Laurent Hirsinger, and Michel Devel, Computation of flexoelectric coefficients of a MoS₂ monolayer with a model of self-consistently distributed effective charges and dipoles, *J. Chem. Phys.* **156**, 174104 (2022).
- [27] Brahmanandam Javvaji, Bohayra Mortazavi, Xiaoying Zhuang, and Timon Rabczuk, Exploring tensile piezoelectricity and bending flexoelectricity of diamane monolayers by machine learning, *Carbon* **185**, 558 (2021).
- [28] Brahmanandam Javvaji, Xiaoying Zhuang, Timon Rabczuk, and Bohayra Mortazavi, Machine-learning-based exploration of bending flexoelectricity in novel 2D van der Waals bilayers, *Adv. Energy Mater.* **12**, 2201370 (2022).
- [29] M. Royo and M. Stengel, First-principles theory of spatial dispersion: Dynamical quadrupoles and flexoelectricity, *Phys. Rev. X* **9**, 021050 (2019).
- [30] Aldo H. Romero *et al.*, ABINIT: Overview and focus on selected capabilities, *J. Chem. Phys.* **152**, 124102 (2020).
- [31] Miquel Royo and Massimiliano Stengel, Lattice-mediated bulk flexoelectricity from first principles, *Phys. Rev. B* **105**, 064101 (2022).
- [32] M. Springolo, M. Royo, and M. Stengel, Direct and converse flexoelectricity in two-dimensional materials, *Phys. Rev. Lett.* **127**, 216801 (2021).
- [33] I. Naumov, A. M. Bratkovsky, and V. Ranjan, Unusual flexoelectric effect in two-dimensional noncentrosymmetric sp^2 -bonded crystals, *Phys. Rev. Lett.* **102**, 217601 (2009).
- [34] K.-A. N. Duerloo and E. J. Reed, Flexural electromechanical coupling: A nanoscale emergent property of boron nitride bilayers, *Nano Lett.* **13**, 1681 (2013).
- [35] Massimo V. Fischetti and William G. Vandenberghe, Mermin-wagner theorem, flexural modes, and degraded carrier mobility in two-dimensional crystals with broken horizontal mirror symmetry, *Phys. Rev. B* **93**, 155413 (2016).
- [36] Tue Gunst, Kristen Kaasbjerg, and Mads Brandbyge, Flexural-phonon scattering induced by electrostatic gating in graphene, *Phys. Rev. Lett.* **118**, 046601 (2017).
- [37] Samuel Poncé, Miquel Royo, Marco Gibertini, Nicola Marzari, and Massimiliano Stengel, Accurate prediction of Hall mobilities in two-dimensional materials through gauge-covariant quadrupolar contributions, *Phys. Rev. Lett.* **130**, 166301 (2023).
- [38] Samuel Poncé, Miquel Royo, Massimiliano Stengel, Nicola Marzari, and Marco Gibertini, Long-range electrostatic contribution to electron-phonon couplings and mobilities of two-dimensional and bulk materials, *Phys. Rev. B* **107**, 155424 (2023).
- [39] Yuanjun Zhou, K. M. Rabe, and David Vanderbilt, Surface polarization and edge charges, *Phys. Rev. B* **92**, 041102(R) (2015).
- [40] Manfredo P. Do Carmo, *Differential Geometry of Curves and Surfaces*, 2nd ed. (Courier Dover Publications, Mineola, New York, 2016).
- [41] M. Stengel, Flexoelectricity from density-functional perturbation theory, *Phys. Rev. B* **88**, 174106 (2013).
- [42] See Supplemental Material at <http://link.aps.org/supplemental/10.1103/PhysRevLett.131.236203> for more information about theoretical derivations, computational details, and results, which includes Refs. [43–50].
- [43] M. Stengel, Microscopic response to inhomogeneous deformations in curvilinear coordinates, *Nat. Commun.* **4**, 2693 (2013).
- [44] Massimiliano Stengel and David Vanderbilt, First-principles theory of flexoelectricity, in *Flexoelectricity in Solids From Theory to Applications*, edited by Alexander K. Tagantsev and Petr V. Yudin (World Scientific Publishing Co., Singapore, 2016), Chap. 2, pp. 31–110.
- [45] D. R. Hamann, Optimized norm-conserving Vanderbilt pseudopotentials, *Phys. Rev. B* **88**, 085117 (2013).
- [46] M. J. van Setten, M. Giantomassi, E. Bousquet, M. J. Verstraete, D. R. Hamann, X. Gonze, and G.-M. Rignanese, The PseudoDojo: Training and grading a 85 element optimized norm-conserving pseudopotential table, *Comput. Phys. Commun.* **226**, 39 (2018).
- [47] K. S. Novoselov, A. Mishchenko, A. Carvalho, and A. H. Castro Neto, 2D materials and van der Waals heterostructures, *Science* **353**, aac9439 (2016).
- [48] S. M. Nakhmanson, A. Calzolari, V. Meunier, J. Bernholc, and M. Buongiorno Nardelli, Spontaneous polarization and piezoelectricity in boron nitride nanotubes, *Phys. Rev. B* **67**, 235406 (2003).
- [49] Songsong Zhou, Jian Han, Shuyang Dai, Jianwei Sun, and David J. Srolovitz, van der Waals bilayer energetics: Generalized stacking-fault energy of graphene, boron nitride, and graphene/boron nitride bilayers, *Phys. Rev. B* **92**, 155438 (2015).
- [50] Peter G. Steeneken, Robin J. Dolleman, Dejan Davidovikj, Farbod Aljani, and Herre S. J. van der Zant, Dynamics of 2D material membranes, *2D Mater.* **8**, 042001 (2021).
- [51] Gonze *et al.*, ABINIT: First-principles approach to material and nanosystem properties, *Comput. Phys. Commun.* **180**, 2582 (2009).
- [52] Miquel Royo and Massimiliano Stengel, Exact long-range dielectric screening and interatomic force constants in quasi-two-dimensional crystals, *Phys. Rev. X* **11**, 041027 (2021).
- [53] R. S. Pease, An x-ray study of boron nitride, *Acta Crystallogr.* **5**, 356 (1951).
- [54] Bo Wang, Yijia Gu, Shujun Zhang, and Long-Qing Chen, Flexoelectricity in solids: Progress, challenges, and perspectives, *Prog. Mater. Sci.* **106**, 100570 (2019).
- [55] Javier Junquera, Yousra Nahas, Sergei Prokhorenko, Laurent Bellaiche, Jorge Íñiguez, Darrell G. Schlom, Long-Qing Chen, Sayeef Salahuddin, David A. Muller, Lane W. Martin, and R. Ramesh, Topological phases in polar oxide nanostructures, *Rev. Mod. Phys.* **95**, 025001 (2023).

- [56] Daniel Bennett, Gaurav Chaudhary, Robert-Jan Slager, Eric Bousquet, and Philippe Ghosez, Polar meron-antimeron networks in strained and twisted bilayers, *Nat. Commun.* **14**, 1629 (2023).
- [57] Jiantian Zhang, Weina Zhao, Peng Yu, Guowei Yang, and Zheng Liu, Second harmonic generation in 2D layered materials, *2D Mater.* **7**, 042002 (2020).
- [58] G. Kresse and J. Hafner, *Ab initio* molecular dynamics for liquid metals, *Phys. Rev. B* **47**, 558 (1993).
- [59] G. Kresse and J. Hafner, *Ab initio* molecular-dynamics simulation of the liquid-metal–amorphous-semiconductor transition in germanium, *Phys. Rev. B* **49**, 14251 (1994).
- [60] G. Kresse and J. Furthmüller, Efficiency of *ab-initio* total energy calculations for metals and semiconductors using a plane-wave basis set, *Comput. Mater. Sci.* **6**, 15 (1996).
- [61] G. Kresse and D. Joubert, From ultrasoft pseudopotentials to the projector augmented-wave method, *Phys. Rev. B* **59**, 1758 (1999).